# The Investigation of Atmospheric Angular Momentum as a Contributor to Polar Wobble and Length of Day Change with AMIP II GCM Data[1]

Zhong Min (钟 敏)[1,2], Yan Haoming (闫昊明)[1], and Zhu Yaozhong (朱耀仲)[1,2]

[1] *Institute of Geodesy and Geophysics, Chinese Academy of Sciences, Wuhan* 430077

[2] *LASG, Institute of Atmospheric Physics, Chinese Academy of Sciences, Beijing* 100029

(Received March 15, 2001; revised January 5, 2002)

ABSTRACT

The atmospheric angular momentum (AAM) functions in terms of contribution to polar wobble and length of day change, are calculated from the output data of GSM9603 global circulation model (GCM) of Japan Meteorological Agency (JMA), from the reanalysis data of the National Centers for the Environmental Prediction (NCEP) / National Center for Atmospheric Research (NCAR), and from the operational objective analysis data of JMA, respectively. The comparison shows that during the period from 1985 to 1995, the values of the pressure terms in the equatorial components of AAM functions calculated from three data sets agree with each other better along 90°E longitude than along Greenwich meridian direction. The axial component of relative AAM function estimated from GSM 9603 agrees well with those from the other two data sets in terms of seasonal variations with the moderate amplitudes, but not so well with the composite axial component of relative AAM functions estimated from 23 GCM models anticipating in the first phase of AMIP. In addition, its interannual variation from 1979 to 1996 shows the main characteristics of ENSO evolution, just as does the axial component of relative AAM function estimated from NCEP reanalysis data except for the period of anomalous ENSO from 1991 to 1993.

**Key words:** Atmospheric Model Inter-comparison Project (AMIP), Atmospheric Angular Momentum (AAM), Earth rotation

## 1. Introduction

In the discussion of atmospheric contributions to Earth' rotational variations, the AAM functions are composed of three components: two equatorial components as the major sources exciting polar wobble from sub-seasonal to interannual time scale and one axial component exciting more than 90% seasonal length of day changes (Barnes et al. 1983). Each component consists of wind term, and pressure term due to the atmospheric mass redistribution. Although all the four meteorological centers around the world use the same meteorological data as the inputs in their four-dimensional data assimilation (4DDA) systems, the estimated AAM functions present different behaviors (Hide et al. 1997). Eubanks et al. (1988), for instance, found that based on two data sets (NCEP and JMA), the correlation

[1] This work was supported by the National Natural Science Foundation of China under Grant Nos. 49904002 and 40074004, the National Climbing Project of China under Grant No. 970231003, and LASG, Institute of Atmospheric Physics, Chinese Academy of Sciences.

is higher than 0.9 between two pressure terms, but lower than 0.4 between two wind terms in the equatorial component of AAM functions. The disagreement in the wind terms may be partly due to the lack of data in sparse regions, such as the South Pacific (Eubanks et al. 1988), and partly due to the different methods in the 4DDA systems (Eubanks et al. 1993). However, Aoyama and Naito (2000) argued that the disagreement mainly results from different vertical wind integration methods between NCEP and JMA, since NCEP integrates wind from 1000 hPa to the top level (Rosen and Salstein 1985), while JMA from mountainous surface pressures to 10 hPa (Naito et al. 1987). Even with the same wind integrating method, the contributions of equatorial tropospheric wind estimated from JMA data set and NCEP data set are still discrepant due to the different tropospheric regional winds associated with the Asian monsoon (Aoyama and Naito 2000).

In the second phase of Atmospheric Model Inter-comparison Project (AMIP II), 30 modeling groups around the world were required to simulate the evolution of the climate from 1979 to 1996, with the same observed monthly average global sea surface temperature and sea ice distributions as boundary conditions (Gates et al. 1999). Hence in this paper atmospheric angular momentum functions are calculated based on 1979–1996 data of GSM9603 GCM with emphasis on the different wind contributions to the wobble by different wind integration methods. Section 2 briefly presents the three-dimensional atmospheric angular momentum model in use. Section 3 outlines the data and methodology. The comparisons of pressure terms and wind terms are shown in section 4 in terms of seasonal and interannual variations, based on the datasets of NCEP / NCAR, JMA and GSM9603 GCM. A summary is given in section 5.

## 2. Atmospheric angular momentum model

The variation in the orientation of Earth's rotational axis with respect to Earth's figure axis is called polar wobble, and Earth's axial fluctuations as changes in length of day (LOD). In the absence of external torque, the Earth including the fluid parts conserves its angular momentum. So mass redistributions and torque of geophysical fluids such as atmosphere, ocean, and land water over the solid-Earth can cause the wobble and the LOD change (Munk and Macdonald 1960; Lambeck 1980). In Earth's fixed reference frame, the wobble and LOD changes can be generally expressed by the following perturbation equations for equatorial and axial components of angular velocities, respectively (Barnes et al. 1983; Eubanks 1993).

$$\tilde{m} + \frac{\mathrm{i}}{\tilde{\sigma}_c}\frac{d\tilde{m}}{dt} = \tilde{\chi} \ , \tag{1}$$

$$\frac{d}{dt}(m_3 + \chi_3) = 0 \ . \tag{2}$$

In Eq.(1) $\tilde{m} = m_1 + \mathrm{i}m_2$ is a dimensionless complex-valued small quantity representing the equatorial angular velocities for the wobble, and $\tilde{\sigma}_c$ is the complex frequency of Chandler wobble. In Eq.(2) $m_3$ is a dimensionless small quantity representing the axial angular velocity for the LOD change with a relation $m_3 = -\Delta\Lambda / \Lambda_0$, where $\Lambda_0$ and $\Delta\Lambda$ are a standard LOD and its deviation, respectively. The properties $\chi_1$ and $\chi_2$ in $\tilde{\chi} = \chi_1 + \mathrm{i}\chi_2$ of Eq.(1) and $\chi_3$ in Eq.(2) are, respectively, the equatorial and axial angular momentum functions of geophysical fluids and tidal torque. The angular momentum functions, associated with atmospheric mass

redistribution and wind field, are known as atmospheric angular momentum (AAM) functions with $\chi_1$ as Greenwich meridian component and $\chi_2$ as 90°E meridian component. For atmospheric pressure terms, the variation of $\chi_1$ ($\chi_2$) component is mainly caused by the atmospheric mass redistributions over ocean (continental) regions. The axial and equatorial principal moments of mantle and the transfer functions are adjusted to the values given by Eubanks (1993), in the estimations of the AAM functions with the GSM9603, NCEP and JMA data in this study (see the appendix for more detail and also see Aoyama and Naito 2000).

## 3. Data and methodology

### 3.1 *GSM9603 model description*

GSM9603 (T63 L30H) consists of an atmospheric general circulation model and a land surface process developed at JMA, anticipating the second phase of Atmospheric Model Inter-comparison Project (AMIP II). The simulation is performed according to AMIP requirement from January 1979 to February, 1996 with uniform boundary conditions of monthly sea ice extent and observed sea surface temperature (SST) from January 1979 to February, 1996. The values of the atmospheric $CO_2$ concentration and the solar constant are fixed at 348 ppmv and 1365 W $m^{-2}$, respectively. The monthly mean upper air data are interpolated onto the 17 WMO standard pressure levels with top of atmosphere reaches at 10 hPa, and 8 of 17 levels above 100 hPa. The interpolated horizontal resolutions are $2.5^\circ \times 2.5^\circ$ in latitudinal and longitudinal directions with the interpolation done at every sampled time step (e.g., every time step for temperature tendencies, and every six hours for winds, etc).

### 3.2 *Archived AAM functions*

For comparison, JMA operational analysis data twice a day from 1985 to 1995 and NCEP reanalysis data four times a day from 1979 to 1999, are applied to the calculation of AAM functions, respectively. Then the functions are converted into monthly series in order to compare with the monthly AAM functions calculated from the GSM9603 data. In the calculation of AAM functions, the wind terms are obtained by integrating winds from mountainous surface pressure to 10 hPa (SP method) with JMA data but from 1000 hPa to 10 hPa (BP method) with NCEP data (see Aoyama and Naito 2000, for details).

### 3.3 *Computation and analysis*

In the computation of AAM pressure terms, the mountainous surface pressures are estimated by a cubic non-periodic spline method based on the hydrostatic equation with $2.5^\circ \times 2.5^\circ$ latitude-longitude grids topography, sea-level pressures and geo-potential heights data (Naito et al. 1987). In the inverted barometer (IB) case, the pressure term of AAM is associated with the isostatical response of ocean to atmospheric pressure variation, while in the non-IB (NIB) case, the oceans are assumed to be rigid.

## 4. Results and discussions

The least square fitting of sinusoids is applied to study the seasonal variations of monthly AAM functions (Table 1). The coefficients of cos terms and sin terms for the annual and semi-annual sinusoids are determined based on the AAM functions with their trends with fourth-order polynomial functions for axial component and linear functions for equatorial

component. The initial phase angles are the first of January under cosine convention.

**Table 1.** Estimated seasonal variations of the amplitudes and phases of AAM functions from 1985 to 1995

| **Annual Variation** | $\chi_1$ Amp ($\times 10^{-8}$) | Phase (°) | $\chi_2$ Amp ($\times 10^{-8}$) | Phase (°) | $\chi_3$ Amp ($\times 10^{-8}$) | Phase (° |
|---|---|---|---|---|---|---|
| Atmospheric NIB−Pressure | | | | | | |
| GSM9603 | 12.60 ± 0.13 | 185.1 ± 5.1 | 24.30 ± 0.95 | 171.4 ± 3.0 | 0.28 ± 0.08 | 205.8 ± 5.8 |
| NCEP | 10.20 ± 1.50 | 215.3 ± 1.4 | 20.41 ± 0.80 | 169.7 ± 3.2 | 0.64 ± 0.06 | 247.6 ± 2.3 |
| JMA | 8.74 ± 1.55 | 220.6 ± 7.6 | 21.04 ± 0.90 | 172.4 ± 3.2 | 0.64 ± 0.07 | 239.8 ± 1.6 |
| Atmospheric IB−Pressure | | | | | | |
| GSM9603 | 5.57 ± 0.31 | 174.0 ± 3.9 | 15.92 ± 0.51 | 172.9 ± 2.4 | 0.30 ± 0.03 | 175.9 ± 5.9 |
| NCEP | 3.42 ± 0.30 | 179.0 ± 5.2 | 13.87 ± 0.42 | 178.4 ± 1.8 | 0.49 ± 0.03 | 215.3 ± 0.7 |
| JMA | 3.33 ± 0.34 | 186.4 ± 4.7 | 14.95 ± 0.45 | 179.0 ± 1.8 | 0.54 ± 0.04 | 206.1 ± 1.3 |
| Atmospheric Wind | | | | | | |
| GSM9603 (BP) | 1.56 ± 0.28 | 10.3 ± 7.1 | 1.60 ± 0.24 | 183.5 ± 7.6 | 4.41 ± 0.32 | 23.3 ± 1.6 |
| GSM9603 (SP) | 0.38 ± 0.15 | 335.9 ± 56.8 | 0.68 ± 0.20 | 165.2 ± 28.1 | 4.39 ± 0.32 | 23.3 ± 1.7 |
| NCEP (BP) | 1.97 ± 0.28 | 27.9 ± 2.5 | 0.76 ± 0.19 | 182.8 ± 13.0 | 4.67 ± 0.29 | 35.6 ± 0.6 |
| JMA (SP) | 4.16 ± 0.64 | 38.4 ± 1.0 | 2.14 ± 0.57 | 32.5 ± 3.4 | 4.89 ± 0.30 | 33.4 ± 0.7 |
| **Semiannual Variation** | | | | | | |
| Atmospheric NIB−Pressure | | | | | | |
| GSM9603 | 2.96 ± 1.13 | 94.8 ± 26.0 | 4.21 ± 1.00 | 354.2 ± 16.9 | 0.33 ± 0.05 | 279.5 ± 11.2 |
| NCEP | 2.94 ± 1.04 | 177.9 ± 21.6 | 3.58 ± 0.99 | 359.6 ± 16.0 | 0.14 ± 0.04 | 93.0 ± 20.5 |
| JMA | 3.01 ± 0.99 | 174.6 ± 22.7 | 2.85 ± 1.14 | 5.7 ± 18.8 | 0.13 ± 0.04 | 98.7 ± 25.4 |
| Atmospheric IB−Pressure | | | | | | |
| GSM9603 | 1.23 ± 0.48 | 57.4 ± 4.9 | 3.73 ± 0.80 | 30.4 ± 3.2 | 0.15 ± 0.02 | 290.5 ± 14.8 |
| NCEP | 1.54 ± 0.35 | 79.2 ± 9.0 | 3.63 ± 0.59 | 29.8 ± 2.5 | 0.08 ± 0.02 | 104.0 ± 20.5 |
| JMA | 1.48 ± 0.38 | 75.4 ± 8.6 | 3.53 ± 0.64 | 32.0 ± 2.4 | 0.07 ± 0.01 | 122.6 ± 30.8 |
| Atmospheric Wind | | | | | | |
| GSM9603 (BP) | 0.18 ± 0.28 | 257.9 ± 59.9 | 0.97 ± 0.30 | 63.3 ± 6.0 | 2.93 ± 0.34 | 233.9 ± 11.1 |
| GSM9603 (SP) | 0.46 ± 0.13 | 333.2 ± 48.1 | 0.97 ± 0.38 | 54.7 ± 3.9 | 2.93 ± 0.34 | 233.6 ± 11.0 |
| NCEP (BP) | 0.43 ± 0.19 | 275.1 ± 30.1 | 0.33 ± 0.19 | 86.4 ± 29.3 | 2.57 ± 0.26 | 253.9 ± 3.2 |
| JMA (SP) | 0.73 ± 0.15 | 301.4 ± 49.0 | 0.40 ± 0.51 | 16.0 ± 39.9 | 2.55 ± 0.27 | 253.6 ± 3.3 |

* GSM9603, NCEP and JMA denote the three data sources, respectively. BP and SP indicate the two different wind integration methods used in this study. The initial phase angles are the first of January. The errors in the table are the least squares fitting errors.

### 4.1 *Atmospheric equatorial angular momentum functions*

The combined effects of the mass redistribution (IB case) and the associated motion (BP case) are represented by $\chi_1^{PIB+w}$ and $\chi_2^{PIB+w}$. The contributions of these effects to the variations of the equatorial component of AAM functions are shown in Fig. 1 based on 1985−1995 GSM9603 data set. The comparisons indicate that the correlation between GSM9603 and NCEP in terms of seasonal variation of equatorial AAM functions $\chi_2^{PIB+w}$ is higher than that in terms of $\chi_1^{PIB+w}$. The main reason is the over−estimated annual variation of pressure term $\chi_1^{PIB}$ with an amplitude of $5.57 \times 10^{-8}$, which is obviously different from $3.42 \times 10^{-8}$ by NCEP and $3.33 \times 10^{-8}$ by JMA. A detail investigation reveals that in both NIB and IB cases, the effective projection $(\cos\lambda + i\sin\lambda)\sin 2\varphi$ of $\chi_1$ component is mainly located over most ocean regions. This indicates that atmospheric mass redistribution has a dominant contribution to the pressure terms of $\chi_1$ component. Therefore, GSM9603 model needs to improve the

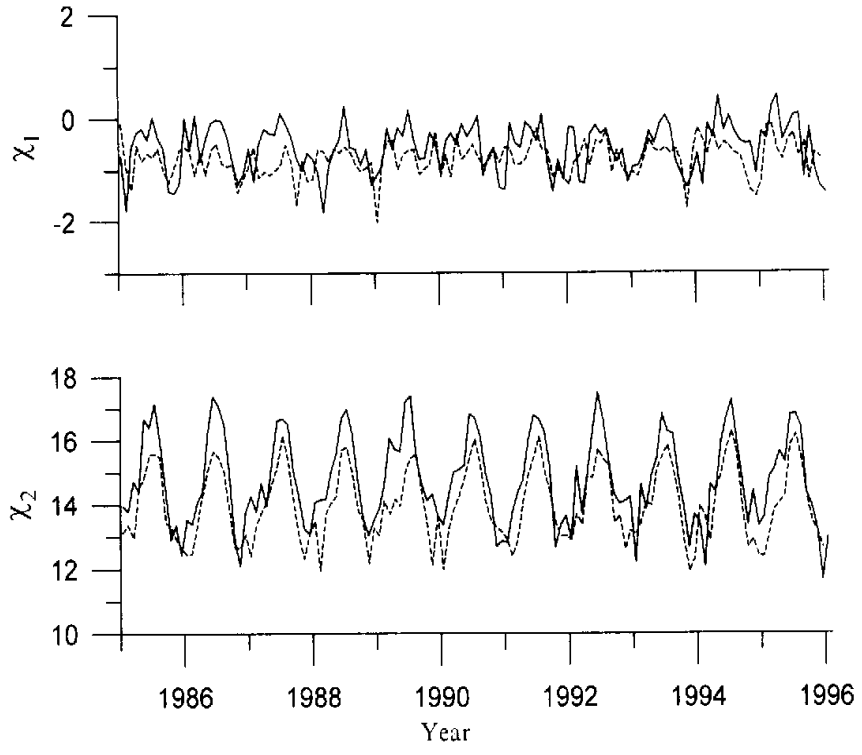


Fig. 1. The equatorial AAM functions $\chi_1^{PIB-}$, $\chi_2^{PIB+}$ estimated from GSM9603 data (solid line) and NCEP reanalysis data (dashed line). BP method is applied for wind terms. The units of $\chi_1$ and $\chi_2$ are all $10^{-8}$ radian.

atmospheric surface mass redistribution over ocean regions.

In contrast, the seasonal variations of $\chi_2^{PIB}$ with annual amplitude and phase ($15.92 \times 10^{-8}$, 172.9°) shown by GSM9603 model agree well with those of NCEP ($13.87 \times 10^{-8}$, 178.4°) and JMA ($14.95 \times 10^{-8}$, 179.0°) (Table 1). The agreement also shows in the semi-annual amplitude and phase ($3.73 \times 10^{-8}$, 30.4°) from GSM9603, ($3.63 \times 10^{-8}$, 29.8°) from NCEP and ($3.53 \times 10^{-8}$, 32.0°) from JMA. This agreement is mainly due to the contribution of mass redistribution to the $\chi_2$ component over Eurasian and North American continent areas. These analyses are also consistent with yearly mean seasonal patterns (Fig. 2), in which the median of each month is estimated from its annual monthly time series during the decade of 1985 to 1995.

As for the different wind contributions caused by different wind integration methods (BP and SP), the annual amplitude of $\chi_1$ ($\chi_2$) estimated by BP method is $1.56 \times 10^{-8}$($1.60 \times 10^{-8}$), much larger than $0.38 \times 10^{-8}$ ($0.68 \times 10^{-8}$) with the same data set of GSM9603 by SP method. However, the semi-annual amplitude of $\chi_1$ by BP method is $0.18 \times 10^{-8}$, smaller than $0.46 \times 10^{-8}$ by SP method. For $\chi_2$ component, the semi-annual amplitudes, estimated by BP and SP methods, are almost the same.

Now turn to the comparison of wind terms between GSM9603 (BP) and NCEP (BP). Figure 2c shows that annual mean seasonal patterns of GSM9603 and NCEP (BP) are roughly in phase but there exists significant overestimation in semi-annual variation of GSM9603

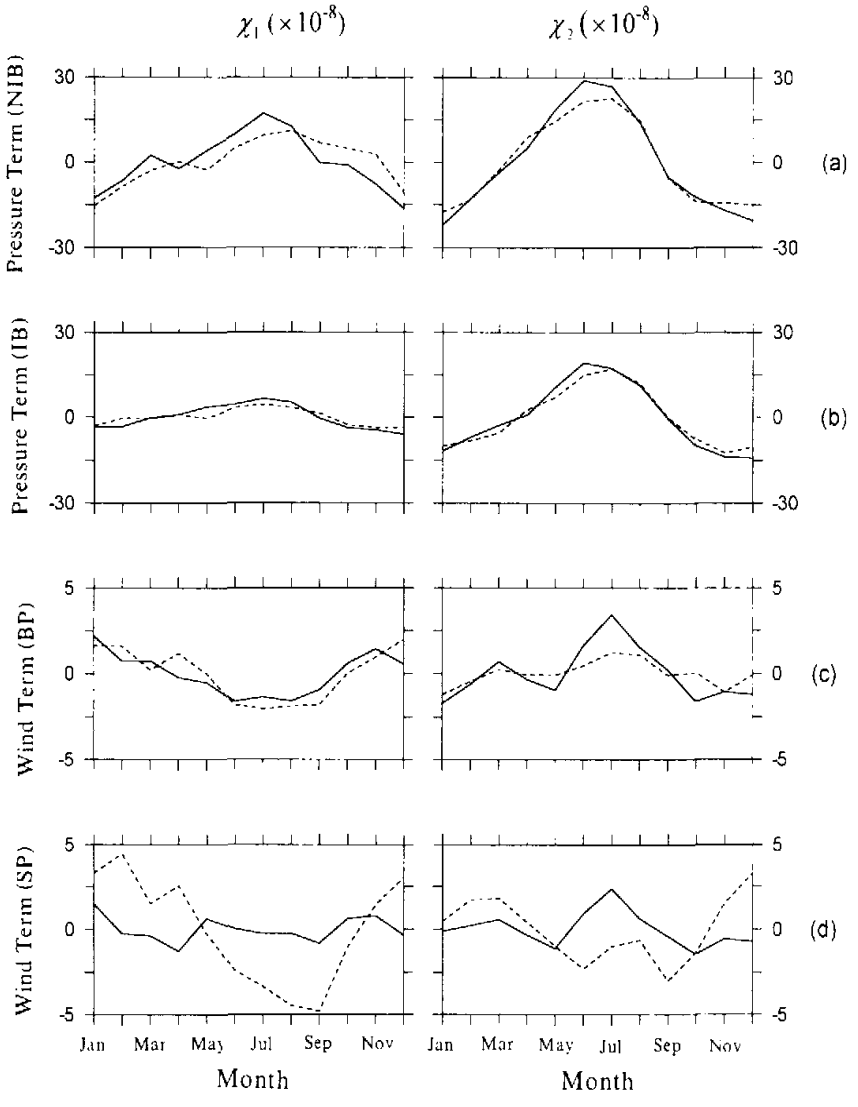


Fig. 2. Comparisons on the seasonal patterns of the equatorial AAM functions. (a) $\chi^{pNIB}$ terms of GSM9603 and NCEP; (b) $\chi^{pIB}$ terms of GSM9603 and NCEP; (c) $\chi^{w}$ (BP) terms of GSM9603 and NCEP; (d) $\chi^{w}$ (SP) terms of GSM9603 and JMA. The GSM9603 results are represented by solid lines. The NCEP and JMA results are indicated by dashed lines.

$\chi_2$ wind term. Figure 2d shows that there remain large disagreements in seasonal patterns between GSM9603 (SP) and JMA (SP). The annual amplitude and phase of $\chi_1$ ($\chi_2$) estimated by BP method are $4.16 \times 10^{-8}$ and 38.4° ($2.14 \times 10^{-8}$ and 32.5°) based on JMA data, and $0.38 \times 10^{-8}$ and 335.9° ($0.68 \times 10^{-8}$ and 165.2°) based on GSM9603 data. In general, the similarity is more obvious between the equatorial relative AAM functions calculated from the same BP method but different data sets (GSM9603 and NCEP) than those calculated with the same da-

ta set GSM9603 but different methods (BP and SP). It suggests that there is still room for the improvement of wind integration methods.

4.2 *Atmospheric axial angular momentum functions*

The seasonal cycle of axial AAM is mainly caused by the asymmetry land–ocean distributions in the northern and southern hemispheres, so there exist different seasonal changes of subtropical jet in the northern and southern hemispheres (Rosen et al. 1991b). This suggests that GSM9603 model generally well simulates the seasonality of subtropical jets in both hemispheres. To verify this thought, seasonal variation of relative AAM calculated with GSM9603 data are compared with that calculated with NCEP data. The comparison shows that the annual amplitude and phase of wind contribution $\chi_3^w$ are $4.41 \times 10^{-9}$ and 23.3° from GSM9603, which agree quite with $4.67 \times 10^{-9}$ and 35.6° from NCEP. The same agreement also appears in the semi–annual amplitude and phase with ($2.93 \times 10^{-9}$, 233.9°) from GSM9603 and ($2.57 \times 10^{-9}$, 253.9°) from NCEP. In addition, the magnitude of semi–annual variation is also significantly better simulated by GSM9603 than by some models in AMIP I. For instance, the semi–annual amplitude of wind term $\chi_3^w$ estimated by the COAGCM model is $4.70 \times 10^{-9}$ (Zhong et al. 2002). Based on the mean result of the 23 models in AMIP I, Hide et al. (1997) points out that the large model errors are caused by misplacing subtropical jets in both hemispheres. Therefore, our results indicate that not only the strength but also the positions of the subtropical jets associated with the seasonal relative AAM variations, are better reproduced by the GSM9603 model, especially in semi–annual cycle.

In the phase comparison, the peak of annual component appears in late January and the peak of semi–annual component in late April. They are all approximately 10 days ahead of those estimated from NCEP reanalysis data. This suggests that phase shifts are still an issue in the simulation of GSM9603 model.

The period from 1979 to 1996 includes two normal ENSO events (1982–1983 and 1986–1987), three abnormal ENSO events (1991 to 1995). It is intriguing to see how well GSM9603 model can handle the ENSO event. Figure 4 shows band–pass filtered variations

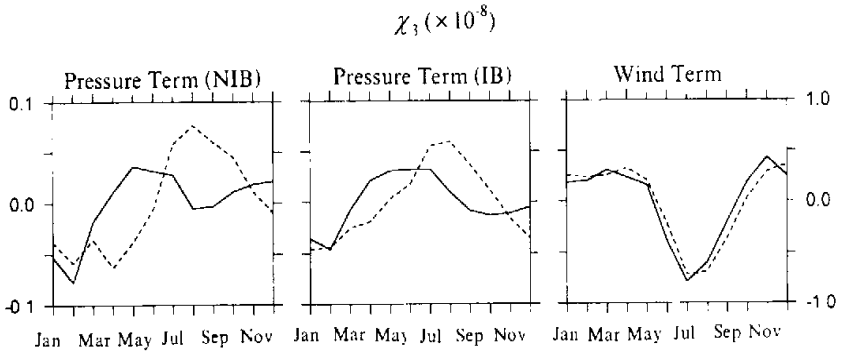


Fig. 3. Comparisons of the seasonal patterns of the axial AAM functions of GSM9603 (solid line) and NCEP (dashed line).

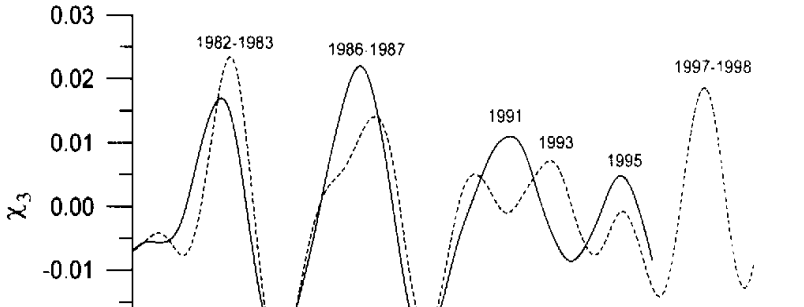


Fig 4 The interannual variations of the axial relative AAM functions, GSM9603 (solid line) and NCEP (dashed line). The unit of $\chi_3$ is $10^{-7}$ radian.

of the axial relative AAM functions at interannual scale, simulated by GSM9603 and estimated from NCEP reanalysis data. In general, GSM9603 reproduces the interannual anomaly series fairly well, except for the period of the two abnormal ENSO events (1991 to 1993). Besides, The underestimation (overestimation) of the amplitude of the 1982–1983 (1986–1987) ENSO signal in AAM noted by Hide et al. (1997) from 23 models in AMIP I, still remain in the simulation of GSM9603. Furthermore, GSM9603 could not distinguish the two abnormal ENSO events (1991 to 1993).

## 5. Conclusion

With 1979–1996 data provided by GSM9603 GCM of Japan Meteorological Agency (JMA), an AMIP II model, the seasonal variations of axial and equatorial components of AAM functions are calculated and compared with those from the reanalysis data of NCEP and the operational analysis data of JMA. These three results agree well with each other in terms of seasonal variation of equatorial component of AAM functions due to mass redistribution along 90°E meridian, but disagree with each other along Greenwich direction. The axial relative AAM function simulated from GSM 9603 are consistent with the other two relative AAM functions in terms of seasonal variations, and better than the composite axial relative AAM functions estimated from 23 AMIP I GCM models. In addition, its interannual variation in the period of normal ENSO similar to that estimated from NCEP reanalysis data, shows the main characteristics of ENSO evolution. With GSM9603 data, the equatorial relative AAM functions are more similar to that estimated from NCEP reanalysis data if the BP method is applied to the wind integration rather than SP method.

APPENDIX

## Atmospheric Angular Momentum Functions

The equatorial ($\chi_1$, $\chi_2$) and axial ($\chi_3$) components of atmospheric angular momentum functions in Eqs.(1) and (2) are given as

$$\begin{aligned}\tilde{\chi} &= \chi_1^P + \chi_1^W + i(\chi_2^P + \chi_2^W) \\ &= \chi_1^P + i\chi_2^P + \chi_1^W + i\chi_2^W \\ &= \frac{-1.098\bar{R}^4}{g(C-A)}\iint p_s \sin\varphi\cos^2\varphi e^{i\lambda} d\lambda d\varphi + \frac{-1.5913\bar{R}^3}{g\Omega(C-A)}\iiint (u\sin\varphi \\ &\quad + iv)\cos^2\varphi e^{i\lambda} dp d\lambda d\varphi \ . \end{aligned} \tag{A1}$$

and

$$\begin{aligned}\chi_3 = \chi_3^P + \chi_3^W &= \frac{0.753\bar{R}^4}{gC_m}\iint p_s \cos^3\varphi d\lambda d\varphi \\ &\quad + \frac{0.998\bar{R}^3}{g\Omega C_m}\iiint u\cos^2\varphi dp d\lambda d\varphi \ . \end{aligned} \tag{A2}$$

Those properties with superscript $P$ such as $\tilde{\chi}^P$ and $\chi_3^P$, indicating the effects of atmospheric mass redistribution, are called pressure terms. While those with superscript W such as $\tilde{\chi}^W$ and $\chi_3^W$, indicating the effects of relative atmospheric angular momentum on the solid Earth, are called wind terms. In (A1) and (A2), $\varphi$, $\lambda$ denote latitude and longitude, respectively, $p_s(\varphi, \lambda, t)$ the atmospheric surface pressure in hPa, $u(\varphi, \lambda, t)$ and $v(\varphi, \lambda, t)$ are the eastward and northward components of the wind at each pressure level, $\bar{R} = 6.37 \times 10^6$ meter is the mean radius of the Earth, $\Omega = 7.292 \times 10^{-5}$ s$^{-1}$ mean rotation rate, and $g = 9.80$ m s$^{-2}$ the mean acceleration due to gravity. The numerical coefficients in equation (A1) and (A2) are the transfer functions defined by Eubanks (1993) in the model. They are introduced to consider the "Love number" corrections for the elastically deformable Earth with respect to the rigid Earth with the assumption of the core–mantle decoupling. The constants $C$ and $C_m$ are the axial principal moments of the Earth and mantle, and $A$ is equatorial principal moment of the Earth. The differences between the transfer functions evaluated by Eubanks (1993) and by Barnes et al. (1983) are shown in Aoyama and Naito (2000).

The authors would like to thank JMA for providing GSM9603 as well as the operational objective data. Thanks are also given to NCEP for providing the reanalysis data.

REFERENCES

Aoyama Y., and I. Naito, 2000: Wind contribution to the Earth's angular momentum budgets in seasonal variation. *J. Geophys. Res.*, **105**, 12417–12432.

Barnes, R. T., H. R. Hide, A. A. White, and C. A. Wilson, 1983: Atmospheric angular momentum fluctuation, length of day changes and polar motion. *Proc. Roy. Soc. London*, **387**(Ser. A), 31–73.

Eubanks, T. M., J. A. Steppe, J. O. Dickey, R. D. Rosen, and D. A. Salstein, 1988: Causes of rapid motions of the Earth's pole. *Nature*, **334**, 115–119.

Eubanks, T. M., 1993: Variation in the orientation of the Earth. *Contribution of Space Geodesy to Geodynamics*,

Geodyn. Ser., AGU, Washington, D. C., **24**, 1–54.

Gross, R. S., and U. J. Lindqwister, 1992: Atmospheric excitation of polar motion during the GIG'91 measurement campaign. *Geophys. Res. Lett.*, **19**, 849–852.

Gates, W. L., J. S. Boyle, and C. Covey, 1999: An overview of the results of the Atmospheric Model Inter-comparison Project (AMIP I). *Bull. Amer. Meteor. Soc.*, **80**, 29–55.

Lambeck, K., 1980: The Earth Variable Rotation, Cambridge Univ. Press, New York, 449pp.

Munk W. H., and G. Macdonald, 1960: The Rotation of the Earth, Cambridge Univ. Press, New York, 323pp.

Naito, I., N. Kikuchi, and K. Yokoyama, 1987: Results of estimating the atmospheric effective angular momentum functions based on the JMA global analysis data. *Publ. Int. Latitude Obs. Mizusawa*, **20**, 1–11.

Hide, R., J. O. Dickey, S. L. Marcus, R. D. Rosen, and D. A. Salstein, 1997: Atmospheric angular momentum fluctuations during 1979–1988 simulated by global circulation models. *J. Geophys. Res.*, **102**, 16423–16438.

Rosen, R. D., D. A. Salstein, and T. M. Wood, 1991b: Zonal contributions to global momentum variations on intra-seasonal through inter-annual timescales. *J. Geophys. Res.*, **96**, 5145–5151.

Rosen, R. D., and D. A. Salstein, 1985: Contribution of stratospheric winds to annual and semiannual fluctuations in atmospheric angular momentum and the length of day. *J. Geophys. Res.*, **90**, 8033–8041.

Rosen, R. D., 1993: The axial momentum balance of Earth and its fluid envelope. *Surv. Geophys.*, **14**, 1–29.

Zhong M., I. Naito, and A. Kitoh, 2002: Atmospheric, oceanic, and hydrologic contributions to annual wobble calculated from COAGCM data. (accepted by *J. Geophys. Res.*).

# 全球大气角动量变化的比较分析

钟 敏 闫昊明 朱耀仲

**摘 要**

利用日本气象局 GSM9603 大气数值模式和客观分析资料以及美国环境预报中心大气再分析数据研究比较全球大气角动量变化。分析表明，三者大气质量再分布角动量东经 90°E 分量的符合程度要好于格林威治方向的分量；而且 GSM9603 对大气轴向相对角动量季节变化的强度模拟与其他两者一致，并明显优于第一阶段 AMIP 23 个大气环流模式的平均模拟结果。另外，GSM9603 大气相对角动量的年际变化基本显示了厄尔尼诺变化的主要历程。

**关键词**：大气环流模式比较计划 AMIP，大气角动量，地球自转